Innate immune signaling in a sponge reveals ancient origin of host-symbiont recognition

Bin Yang[1]†§, Benedict Yuen[1]‡§, Huifang Yuan[1], Bernard M Degnan[1]* and Sandie M Degnan[1]*

[1]Centre for Marine Science and School of the Environment, The University of Queensland; Brisbane 4072, Australia

†Present address: Garvan Institute of Medical Research; Sydney, Australia

§Contributed equally to this study

*Corresponding author. Email: s.degnan@uq.edu.au

*Corresponding author. Email: b.degnan@uq.edu.au

Abstract

Innate immunity in animals functions both to defend against pathogens and to regulate interactions with beneficial microbes. Although these dual roles suggest deep evolutionary roots, it remains unclear whether ancestral functions of the immune system were primarily for protection or for maintaining symbiotic partnerships. Here, we address this question using the marine sponge *Amphimedon queenslandica*, which belongs to an early-branching metazoan lineage, by comparing cellular and transcriptional responses to symbiotic and non-symbiotic bacteria. We show that symbionts are rapidly internalized across the epithelial boundary and elicit a swift and pronounced activation of innate immune transcription factors (TFs), including NF-κB, IRF, and STAT, as well as associated pattern recognition receptors (PRRs) and signaling pathways. Both IRF and NF-κB quickly translocate to the nuclei of amoebocytes that are engulfing symbionts, consistent with conserved roles in host–symbiont recognition. In contrast, non-symbiotic bacteria are internalized more slowly and fail to induce comparable immune activation or TF nuclear translocation. These results indicate that the last common ancestor of sponges and other animals already possessed a complex innate immune system capable of distinguishing among bacterial partners, suggesting that immune regulation of symbiosis is an ancient feature of animal evolution.

Introduction

The origin and evolution of animals took place in the continual presence of bacteria, which had long inhabited marine environments before the emergence of metazoans. Throughout their evolutionary history, animals have thus interacted continuously with bacteria in relationships that likely ranged from antagonistic to mutualistic. These interactions created an early selective pressure for mechanisms that enabled animals to distinguish beneficial from harmful microbes, in turn shaping the evolution of the innate immune system, the primary function of which is to discriminate self from non-self [1–11]. Consistent with this, all animals have inherited from a common ancestor many conserved components of innate immunity, including transcription factors (TFs), pattern recognition receptors (PRRs), signaling pathways, and core effector responses [3,12–14]. It is generally known that bacterial detection begins with extracellular or cell-surface PRRs that activate TF-mediated gene regulatory networks, ultimately driving appropriate transcriptional responses [11,15–18]. However, it remains unclear whether specific regulatory networks are conserved across the animal kingdom to distinguish among different types of bacterial associations, as the underlying mechanisms are still poorly understood outside of vertebrates [19–21].

In this context, we investigated the cellular responses and molecular pathways used by the marine demosponge *Amphimedon queenslandica* to distinguish its native symbiotic bacteria from foreign, non-symbiotic bacteria. Sponges are simple, sessile suspension feeders that efficiently and continuously pump large volumes of seawater through their bodies by the beating of flagellated choanocytes, each of which bears a microvillar collar that captures bacteria [22,23]. This mode of feeding suggests sponges possesses a constitutively active innate immune system capable of rapidly and differentially responding to diverse classes of filtered bacteria [24] . Like most other sponges, *A. queenslandica* filter feeds on bacteria while simultaneously housing large numbers of bacterial symbionts in the extracellular space adjacent to the choanocytes [10,25] so the need to rapidly distinguish symbionts from non-symbionts is paramount. Together, these ecological features make sponges valuable and experimentally tractable systems for investigating immune mechanisms used for differential handling of

61 bacteria. Further, sponges provide a valuable evolutionary framework to make comparisons
62 with innate immune mechanisms known in vertebrates. Because sponges represent one of the
63 earliest-diverging metazoan lineages, traits shared between sponges, vertebrates, and other
64 parahoxozoans are likely to have been present in their last common ancestor and to have
65 originated more than 700 million years ago.
66
67 Here, we use *A. queenslandica* as an early-branching metazoan model to investigate how
68 animals distinguish between different bacterial partners at the cellular and molecular levels.
69 We exposed actively feeding juvenile sponges to bacteria from different sources, to test the
70 hypothesis that this sponge employs distinct components of innate immunity to recognize and
71 respond to its own symbiotic bacteria, compared with foreign bacteria with which it has no
72 particular association. By integrating transcriptomic and cellular analyses, we identify signaling
73 and regulatory pathways involved in recognizing symbiotic versus foreign bacteria, specifically
74 revealing core roles for the TFs NF-κB, IRF and STAT. Because these same TFs play very similar
75 roles in vertebrate systems, our findings provide insight into the ancient regulation of animal–
76 microbe interactions and illuminate how the innate immune system may have evolved to
77 balance defense and symbiosis at the dawn of animal evolution.
78
79 **Results**
80 ***Amphimedon* hosts a unique and simple symbiotic bacterial community**
81 Sponges have species-specific bacterial communities that differ from surrounding
82 environmental microbes, and tend to be either high or low in complexity and abundance
83 [10,26–28]. *Amphimedon queenslandica* (Fig. 1A, B) has a microbiome that is low in complexity
84 and abundance, dominated through its life cycle by three vertically-inherited symbiotic
85 gammaproteobacteria – hereafter referred to as *AqS1*, *AqS2* and *AqS3* – that together can
86 comprise up to 95% of the microbiome (Fig. 1C) [25,29]. Unhealthy *A. queenslandica*, which are
87 identified in the wild by lower cellular mass and paler coloration (Fig. 1B), support a reduced
88 relative abundance of the core symbionts consistent with microbiome dysbiosis (Fig. 1C and S1
89 Table). The sponge *Rhabdastrella globostellata*, which is co-located with *A. queenslandica* on

90 coral reefs, hosts a very different and more complex bacterial community that does not include
91 *AqS1*, *AqS2* or *AqS3* (Fig. 1C, D and S1 Table).
92

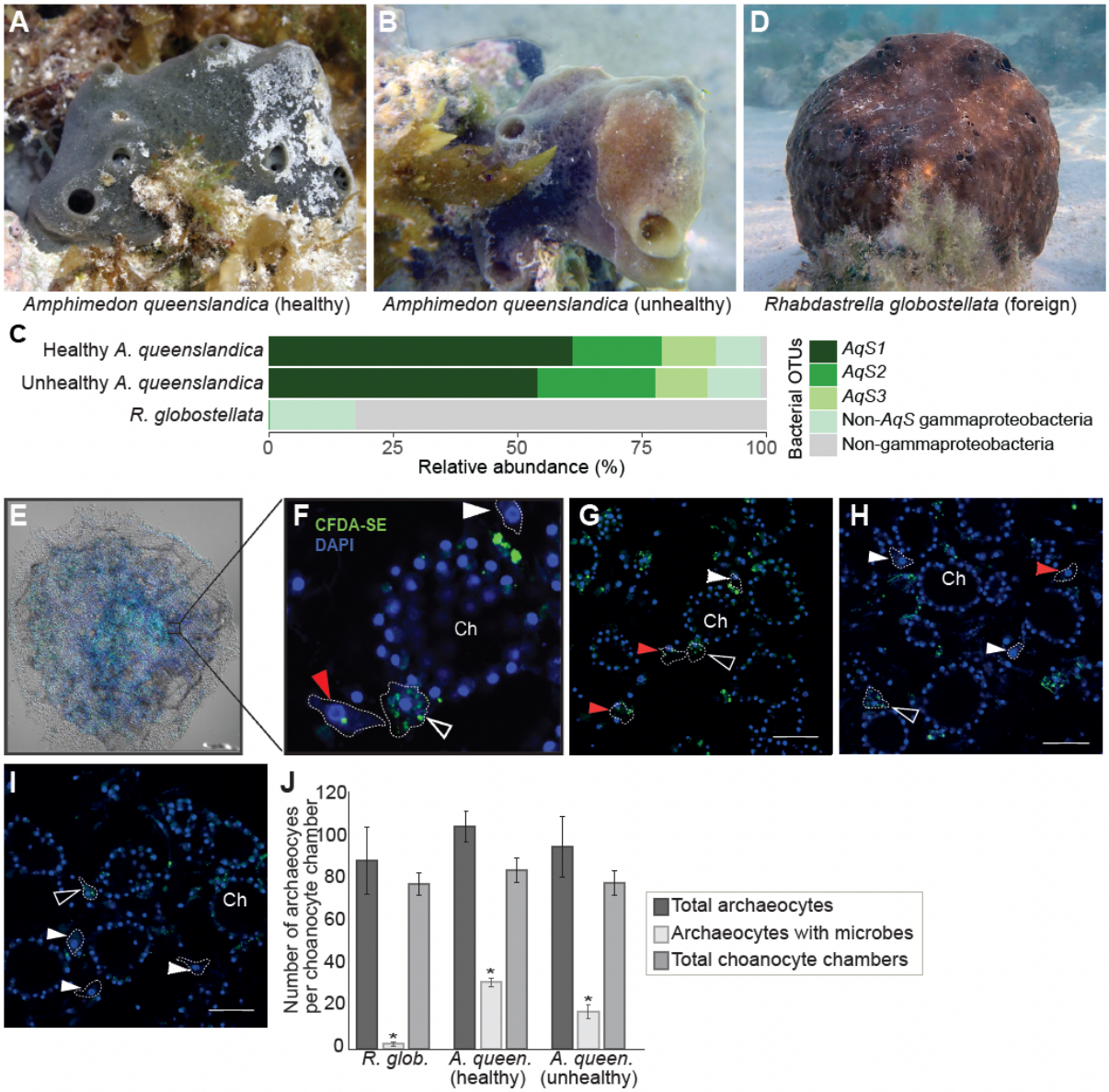

93

94 **Fig. 1. Source and cellular fate of native and foreign microbes in experimental juvenile *A.***
95 ***queenslandica*.** (**A-D**) Microbes inhabiting *Amphimedon queenslandica* and *Rhabdastrella*
96 *globostellata.* (**A**) Healthy and (**B**) unhealthy *A. queenslandica in situ*. (**C**) The relative abundance
97 of symbionts *AqS1*, *AqS2* and *AqS3* and other bacterial operational taxonomic units (OTUs) in
98 healthy and unhealthy *A. queenslandica*, and *R. globostellata* (see S1 Table for taxonomic lists).
99 (**D**) *R. globostellata in situ.* (**E**) DIC and fluorescence micrograph of a DAPI-stained (blue)
100 juvenile fed native bacteria labelled with CFDA-SE (green) at 8 hpe. (**F**) Confocal micrograph of

101 the area surrounding a single choanocyte chamber (Ch) from the same juvenile. Microbes are
102 present in the ring of choanocytes comprising the chamber and a small amoeboid cell adjacent
103 to the chamber (open white arrowhead) and an archaeocyte (red arrowhead). An archaeocyte
104 without labelled microbes is marked with a white arrowhead. These three cells are outlined. (**G-**
105 **I**) Fluorescence micrographs of juveniles at 2 hpe to microbes from healthy (**G**) and unhealthy *A.*
106 *queenslandica* (**H**), and *R. globostellata* (**I**). Microbes are present in choanocyte chambers and
107 small amoebocytes (open white arrowheads) in all three treatments (see S1 and S2 Figs). Scale
108 bars, 25 µm. (**J**) The mean number (± standard error) of total and microbe-containing
109 archaeocytes, and choanocyte chambers in juvenile optical sections from each treatment group
110 (n = 20). Significant differences based in a one-way ANOVA followed by the Tukey's HSD post-
111 hoc test ($p < 0.01$) are denoted an asterisk (*).

112

113 ***Amphimedon* rapidly internalise native bacteria**

114 In addition to an epithelial boundary, which includes numerous chambers of choanocytes,
115 sponges have an internal collagenous mesohyl layer that houses phagocytic, secretory,
116 biomineralizing and stem cells that interact with bacterial food particles and symbionts
117 [22,23,30–33].

118

119 CFDA-SE-labelled bacteria enriched from healthy and unhealthy *A. queenslandica* (referred to
120 hereafter as healthy and unhealthy native bacteria) and from *R. globostellata* (referred to
121 hereafter as foreign bacteria) were introduced separately into 0.2 µm filtered seawater (FSW)
122 surrounding juvenile *A. queenslandica* (Fig. 1E). Within 30 min of exposure, both native and
123 foreign bacteria were present in choanocytes – internal flagellated epithelial cells that draw
124 water through the sponge body and capture bacteria [23,34] – and in amoeboid cells that
125 appear to be in contact with the basal surface of the choanocytes (Fig. 1 and S1 Fig.). By 2 hours
126 post-exposure (2 hpe), only native bacteria had been transferred to archaeocytes, larger
127 phagocytic cells that reside in the internal mesohyl ($p < 0.01$) (Fig. 1G-I). At this time, more
128 archaeocytes contained bacteria from healthy compared to unhealthy *A. queenslandica* ($p <$
129 0.01) (Fig. 1G, H, J and S2 Fig.), suggesting this sponge has a finely tuned capacity to rapidly
130 discern not only native from foreign bacteria but also native communities that differ in content
131 and state.

132

133 **Native symbionts induce a dramatic and transient innate immune response**

134 To characterise the rapid differential response of *A. queenslandica* juveniles to native and
135 foreign bacteria at a molecular level, we compared transcriptomes of juveniles exposed to
136 these bacterial communities for 2 and 8 hours (S2 Table). Principle component analysis (PCA) of
137 biologically-replicated transcriptomes reveals that the sponge has markedly different responses
138 to native and foreign microbes (Fig. 2A). Healthy native bacteria induce a rapid and transient
139 transcriptional response, with about twice as many genes being differentially expressed
140 compared to foreign bacterial treatments (DESeq2, p-adj < 0.05; Fig. 2B-E, S3 Fig. and S3 Table).
141 This rapid transcriptional response largely reverts to pre-exposure (FSW) levels by 8 hpe. This is
142 in stark contrast to the response to foreign bacteria, which is slower, more protracted and
143 comprises a different gene set.

144

145 Bacteria from unhealthy *A. queenslandica* induced similar changes in gene expression
146 compared to healthy native bacteria, except that the transcriptional response is markedly
147 weaker and slower. This muted response correlates with a slower transfer of unhealthy native
148 bacteria to archaeocytes (Fig. 1J) and is consistent with the host sponge being able to recognise
149 subtle differences in its microbiome composition and to attenuate its response accordingly.

150

151 Native bacterial symbionts induce changes in the expression of over 80 TFs within 2 hpe (p-adj <
152 0.05), with most reverting back to pre-exposure transcript levels by 8 hpe (Fig. 2C). This timing
153 correlates with the first transfer of native bacteria to archaeocytes (Fig. 1), indicating these
154 juveniles are poised for a rapid transcriptional response to their native symbionts. These
155 differentially expressed TFs are constitutively enriched in adult epithelial choanocytes and
156 pinacocytes, but are also present in diverse internal mesohyl cell types (S5 Fig. and S5 Table).
157 Choanocytes and pinacocytes are the first cells to contact external bacteria in both juveniles
158 and adults, and these stages have similar gene expression profiles [35,36].

159

160 TFs that are transiently upregulated in response to native symbionts include NF-κB, two IRFs,
161 STAT, two SMADs, AP-1, three Fox genes, a nuclear receptor (NR), and all members of ETS and
162 13 of 17 members of bZIP families. Most of these TFs have known roles in bilaterian innate

immunity. *NF-κB*, *IRF*, *STAT*, *SMAD1/5*, *SMAD3*, *ATF2*, *Oasis A* and *Oasis B* transcript levels induced by bacteria from unhealthy *A. queenslandica* increase more slowly, such that 8 hpe levels are similar to the 2 hpe response to bacteria from healthy individuals (Fig. 2C). This matches the overall prolonged transcriptional response and the slower cellular processing of these bacteria.

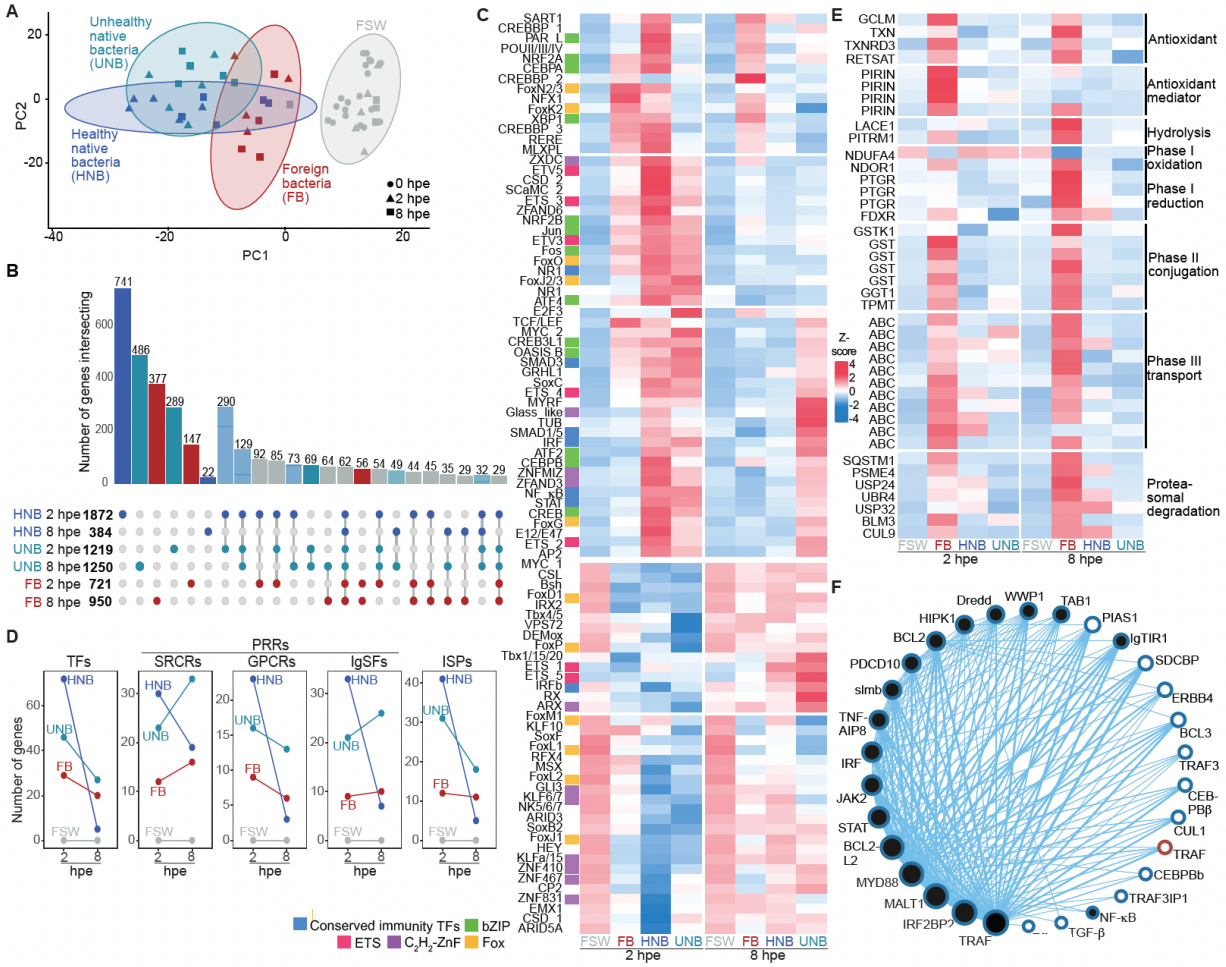

Fig. 2. Rapid and transient induction of immunity genes by native symbionts. (**A**) PCA of transcriptomes from juvenile *A. queenslandica* exposed to FSW (n = 28; grey; 0 hpe controls, circles); foreign bacteria (n = 8; FB, red); native bacteria from healthy (n = 10; HNB, blue) and unhealthy *A. queenslandica* (n = 10; UNB, cyan) at 2 (triangles) and 8 (squares) hpe. 95% confidence ellipses shown. (**B**) UpSet plot summarising the relationship of significantly differentially expressed coding sequences induced by native and foreign bacteria at 2 and 8 hpe relative to FSW (DESeq2; *p*-adj < 0.05). The number of differentially expressed genes in each

178 bacterial treatment is to the left in bold. The number of differentially expressed coding
179 sequences intersecting between treatment groups at the top of each bar. The colour coding
180 follows (A) except for gene intersecting between healthy and unhealthy native bacterial
181 treatment (teal bars). Grey bars, intersections between native and foreign bacteria. (**C**)
182 Hierarchically clustered heatmap of differentially expressed TF genes (*p*-adj < 0.05). TF names
183 are shown to the left. (**D**) Slope charts of the variation in the number of the differentially
184 expressed TFs, PRRs (SRCRs, GPCRs, IgSFs) and immunity signalling pathway components (ISPs)
185 induced by bacterial at 2 and 8 hpe (see S3 Fig. for heatmap of differentially expressed PRRs
186 and ISPs). (**E**) Genes encoding conserved enzymes involved in xenobiotic metabolism activated
187 by foreign bacteria, with phases shown to the right. z-score for C and E shown in the middle. (**F**)
188 Network diagram of the top 30 connected co-expressed genes induced by healthy native
189 bacteria based on WGCNA. The degree of connectivity is indicated by the thickness of the
190 edges/connections. The number of edges is represented by the size of the gene nodes. The
191 nodes with black fill indicate genes identified by sPLS-DA as key differentiators between
192 responses to native symbionts versus foreign bacteria (S4 Fig. and S4 Table). All genes are in
193 WGCNA module 1 (blue), except the TRAF in brown (module 2) (S7 Fig., and S6 and S7 Tables).
194

195 PRR expression induced by native bacteria closely matches that of the TFs and includes the
196 transient differential expression of 56 scavenger receptor cysteine-rich domain-containing
197 (SRCR), 32 G protein-coupled receptor (GPCR) and 50 immunoglobulin superfamily (IgSF) genes
198 (Fig. 2D, S3 Fig. and S3 Table). Two Toll-like receptors, AmqIgTIR1 and 2, which are comprised of
199 extracellular IL1R-like Igs and an intracellular TLR-like Toll/interleukin1 domain [37] are uniquely
200 regulated by native bacteria. Multiple sponge-specific GPCRs with close affinity to
201 parahoxozoan γ-aminobutyric acid (GABA) receptors also are induced. GABA can be synthesised
202 and degraded by *AqS1* and is involved in host-microbe interactions in other animal holobionts
203 (S3 Fig.) [38–40]. By contrast, multiple CL163-L1 SRCRs are upregulated in *A. queenslandica*
204 exposed to foreign bacteria; this SRCR is upregulated in mammalian macrophages during
205 inflammation [41]. Both the GABA- and CL163-like receptors are most highly expressed in
206 epithelial pinacocytes and choanocytes in adults, consistent with these cells constitutively
207 expressing PRRs to detect and discriminate native from foreign bacteria (S5 Fig.).
208

209 Genes encoding conserved members of multiple innate immunity pathways are also transiently
210 activated at 2 hpe by native symbionts from healthy *A. queenslandica*. These include eight
211 TRAFs of the pro-inflammatory cytokine TNF pathway, and multiple components of Toll, Imd,

212 apoptosis, TGF-β and JAK-STAT pathways (Fig. 2D, S3 Fig. and S3 Table). Once again, most of
213 these are expressed constitutively in adult epithelial pinacocytes and choanocytes (S5 and S6
214 Figs and S5 Table).
215
216 There are markedly fewer innate immunity genes induced by foreign bacteria, and these are
217 largely expressed at lower levels and not transiently (Fig. 2, S3 Fig. and S3 Table). In addition to
218 this weaker innate immune response, the prolonged response to foreign bacteria includes the
219 activation of genes involved in xenobiotic metabolism (Fig. 2E). By contrast to innate immunity
220 genes, xenobiotic genes activated by the foreign microbes are chiefly constitutively expressed
221 in internal archaeocytes (S5 Fig. and S5 Table).
222
223 **IRF, NF-κB and STAT appear central to sponge-symbiont interactions**
224 To identify genes most likely to contribute to *A. queenslandica*'s rapid innate immune response
225 to its native bacteria, we combined DESeq2 analyses with a multivariate sparse partial least
226 squares discriminant analysis (sPLS-DA) and a weighted gene co-expression network analysis
227 (WGCNA). Two of the six WGCNA co-expression modules are comprised of genes induced at 2
228 hpe by native symbiotic bacteria, with module 1 including most of the activated immunity
229 genes identified by DESeq2 and sPLS-DA (99% of the sPLS-DA identified genes overlap with
230 DESeq2 identified genes; Fig. 2F, S7 Fig. and S6 Table). The most highly connected genes in this
231 co-expression network are orthologues of bilaterian genes involved in innate immunity,
232 endocytosis and vesicle trafficking, with IRF, NF-κB and STAT being the most connected TFs (Fig.
233 2F). Given this, we generated antibodies against these three TFs to experimentally test their
234 potential roles in regulating immune gene expression when the juvenile contacts its native
235 symbionts.
236
237 IRF, NF-κB and STAT are constitutively localised in the cytoplasm of juvenile choanocytes - IRF is
238 uniquely enriched in the microvillar collar - and proximal ameobocytes (Fig. 3A-D and S8 Fig.).
239 NF-κB is also constitutively nuclear localised in a subset of archaeocytes in the vicinity of
240 choanocyte chambers in juveniles reared in filtered sea water. At 2 hpe, IRF translocates into
241 the nuclei of proximal amoebocytes that have engulfed native bacteria. By contrast, at the

242 same time IRF co-localises with foreign bacteria in the cytoplasm of these cells; there is no
243 evidence of nuclear localisation (Fig. 3E, I). This is consistent with IRF playing a central role in
244 the initial discrimination of native and foreign bacteria. NF-κB co-localises with IRF in nuclei of
245 amoebocytes that have engulfed native bacteria but are no longer in direct contact with
246 choanocyte chambers (Fig. 3F-H, J-L), suggesting NF-κB nuclear localisation occurs after IRF in
247 these cells. At the same time, only native bacteria induce STAT to translocate into the nuclei of
248 a subset of amoebocytes that are not associated with choanocyte chambers and do not appear
249 to have engulfed bacteria (Fig. 3G, H, K, L), suggesting this is occurs by intercellular signalling -
250 JAK-STAT, Toll, Imd, FoxO, Wnt and TGF-β pathway components are upregulated at 2 hpe.
251

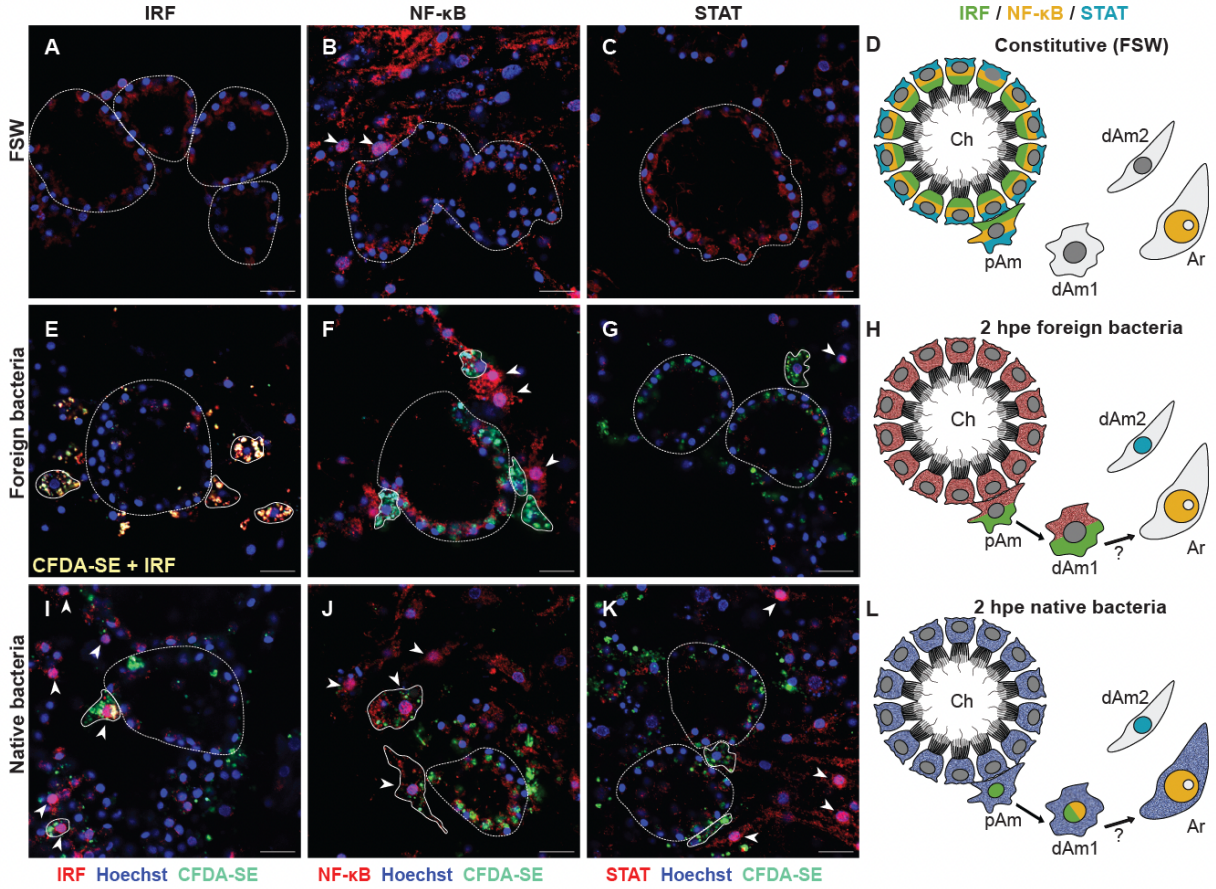

252
253

254 **Fig. 3. Subcellular localization of IRF, STAT, and NF-κB in response to native and foreign**
255 **bacteria.** (**A-D**) Immunostained 2 hpe juveniles exposed to FSW; (**E-H**) foreign bacteria; and (**I-L**)
256 healthy native bacteria (IRF, NF-κB or STAT, red; foreign or native bacteria, green; nuclei, blue):
257 (**A,E,I**) IRF; (**B,F,J**) NF-kB; and (**C,G,K**) STAT. (**D,H,L**) Diagrams of a choanocyte chamber (Ch) with

258 proximal and two distant amoebocyte cell types (pAm, dAm1 and dAm2) and archeocytes (Ar)
259 showing the nuclear localisation of IRF (green), NF-κB (orange) and STAT (blue) in juveniles
260 reared in FSW (**D**), or exposed to foreign bacteria (**H**) or native bacteria (**L**). IRF localisation in
261 the cytoplasm in distal amoebocytes dAM1 is shown in H. Red and blue speckled colouring
262 demarcates the cells housing foreign and native bacteria at 2 hpe, respectively. Arrows and
263 question marks indicate the unknown lineage relationship between amoebocytes to each other
264 and to archaeoctyes, including transdifferentiation [36]. Scale bars, 10 µm.

265

266 **Discussion**

267 The responses of the sponge *Amphimedon queenslandica* to symbiotic and foreign bacteria are
268 markedly different in speed and scale, and provide strong support for the innate immune
269 system being critical in sponge-symbiont interactions. The sponge is poised to rapidly detect
270 and transcriptionally respond to its symbionts, swiftly activating a suite of conserved innate
271 immunity genes. This includes a wide array of TF families that have roles in innate immunity
272 across the animal kingdom, such as IRF, STAT, NF-κB, AP-1 and other bZIPs, ETS, SMADs and NRs
273 [19,21,42–46]. This suggests that the transcriptional regulation of holobiont fidelity by the
274 innate immune system, such as NF-κB and Toll pathway, evolved early in metazoan evolution,
275 and is consistent with the regulation and maintenance of living animal holobionts using a
276 common set of mechanisms. Indeed, given holozoan-bacteria interactions likely predate the
277 evolution of animal multicellularity [3,13,14] and many core immunity TFs are metazoan
278 innovations (e.g. IRF, AP-1, SMAD, and ETS and NR families [47]), the animal innate immune
279 system may have first evolved to maintain symbiotic relationships, and not to protect against
280 pathogens. The muted, yet longer-lasting, activation of these genes by symbionts derived from
281 unhealthy and dying sponges is consistent with the ancestral innate immune system being
282 finely tuned to detect and respond to subtle dysbiotic conditions to maintain a beneficial
283 microbiome. Interestingly, many of these innate immunity TFs also play developmental roles,
284 which may have been co-opted later in metazoan evolution [24,37,48,49].

285

286 Sponges have no gut, nor nerve and muscle cells, but do have an epithelium and underlying
287 phagocytes that are akin, and arguably homologous, to cell types present in other animals
288 [23,30,32,50]. The constitutive expression of many conserved immunity TF, PRR and signalling
289 genes in the epithelium – sponge pinacocytes and choanocytes – and the rapid activation of IRF

290 and NF-κB in adjacent phagocytes is consistent with these cells being poised to discriminate
291 native from foreign bacteria. Given this, and the tight alliance of symbionts and epithelia in
292 disparate animals [1,3,6,51], it appears that the epithelial boundary has been instrumental in
293 rapidly discriminating beneficial, harmful and neutral bacteria, and thus in shaping host-
294 symbiont interactions since before the origin of the gut.
295
296 IRF appears to be central to the differential response of the sponge to native and foreign
297 bacteria, immediately translocating to nuclei of phagocytes only in response to receiving native
298 symbionts from choanocytes. This suggests these cells are primed to discriminate native from
299 foreign bacteria and initiate a transcriptional response. By contrast, IRF remains in the
300 cytoplasm in sponge amoebocytes that have engulfed foreign bacteria, appearing to co-localise
301 with these bacteria as occurs in macrophages and other cell types, where IRF binds to MyD88
302 on the surface of endosomes and has a non-TF signalling role [44,52–54].
303
304 NF-κB translocates into the nuclei of symbiont-carrying amoebocytes shortly after IRF,
305 suggesting it also contributes to regulation of symbiont processing. Indeed, IRFs and NF-κB
306 regulate the swift transcriptional responses in other animal cells upon stimulation of Toll-like
307 receptors and other PRRs [44,55]. Our findings that these two TFs, along with STAT, appear
308 central to the transcriptional response of *A. queenslandica* to its symbionts, suggests that the
309 role of these TFs in discriminating beneficial symbionts from foreign bacteria also evolved
310 before the divergence of sponge and parahoxozoan lineages. Additionally, these amoebocytes
311 appear to have macrophage-like properties and play a role in sponge defence [32,33]
312 suggesting this cell type is also an ancestral conserved feature of sponges and parahoxozoans.
313
314 In conclusion, we have demonstrated that sponges, like more complex animals, express innate
315 immunity TFs, PRRs and signalling pathways to regulate their microbiome. This occurs rapidly
316 and adjacent to the sponge epithelial layer, consistent with the immune system of aquatic
317 filter-feeding animals being poised to rapidly and differentially respond to beneficial symbiotic
318 bacteria. Given the phylogenetic position of sponges, these results also suggest that the earliest

319 animals primarily used the innate immune system to recognize symbionts to maintain holobiont
320 fidelity.
321
322 **Materials and Methods**
323 **Enrichment and characterisation of sponge bacterial communities**
324 *Amphimedon queenslandica* and *Rhabdastrella globostellata* were collected from Heron Reef,
325 Great Barrier Reef, Australia (23◦27'S, 151◦55'E) (Fig. 1A, B, D), and bacterial communities were
326 enriched from individual sponges as previously described [29,56]. The health of *A.*
327 *queenslandica* individuals was visually assessed in the field prior to collection. Healthy
328 individuals were grey and had high cellular mass, while unhealthy individuals had body regions
329 that were pale brown to olive colour and had a lower cell mass and regions of exposed
330 extracellular matrix (Fig. 1A, B). *A. queenslandica* and *R. globostellata* bacterial enrichments
331 were diluted in 0.2 µm filtered sea water (FSW) to approximate final concentration of 10^7
332 cells/ml. DNA was extracted from approximately 10^6 cells of these bacterial enrichments to
333 identify prokaryotic operational taxonomic units (OTUs) via 16S rRNA gene amplicon
334 sequencing as previously described [25]. All field collections were conducted in accordance
335 with Great Barrier Reef Marine Park Authority Permit G16/38120.1 issued to BM Degnan ad SM
336 Degnan.
337
338 **Rearing *A. queenslandica* larvae and juveniles**
339 Naturally-released *A. queenslandica* larvae were collected in larval traps from 25 individuals,
340 pooled and maintained in ambient seawater for 6-8 h before being induced to settle on the
341 coralline alga *Amphiroa fragilissima* [57,58] Within 6 h of settling on *A. fragilissima*, *A.*
342 *queenslandica* postlarvae were detached from the algae and resettled individually onto glass
343 coverslips [36] . These were placed in sterile 24-well plates in 2 ml FSW and reared for 96 h at
344 25°C until reaching the juvenile stage with a functional aquiferous system [59].
345
346 **Labelling and tracing bacteria in juvenile sponges**
347 Bacterial enrichments were centrifuged at 5000 x g for 10 min and resuspended in 1 ml of 5 µM
348 carboxyfluorescein diacetate succinimidyl ester (CFDA-SE; Vybrant, Thermofisher Scientific) in

349 FSW. After incubating for 15 min at room temperature, the cell suspensions were centrifuged at
350 5000 x g for 10 min. The pellets were washed twice in FSW, resuspended in 1 ml FSW and
351 maintained at 4°C in the dark. Juvenile *A. queenslandica* were washed in FSW and the volume
352 of FSW in each well was adjusted to 1.5 ml. 40 µL of the CFDA-SE labelled microbial
353 enrichments from either a healthy or unhealthy *A. queenslandica*, or *R. globostellata* were
354 introduced to the FSW in each well, yielding final concentrations of 2.8, 3.6 or 2.7 × 10^4 cells/ml,
355 respectively. Control treatments were juveniles receiving 40 µl FSW. Juveniles were then
356 cultivated in the presence of the labelled bacteria in the dark. Individual juveniles were fixed
357 0.5, 1, 2 and 8 h post-exposure (hpe) as previously described [60]. For the 8 hpe incubations,
358 the wells were washed once with fresh FSW after 2 h and the juveniles were reared in FSW for
359 the last 6 h. Fixed juveniles were labelled with 4',6-diamidino-2-phenylindole (DAPI; 1:1000,
360 Molecular Probes), mounted in ProLong Gold anti-fade reagent (Molecular Probes) and
361 observed and photographed using a Zeiss LSM 510 META confocal microscope [61].
362
363 The number of choanocyte chambers, archaeocytes and microbe-containing archaeocytes were
364 counted in four randomly-chosen confocal sections obtained from the inner cortex of five
365 juveniles (n = 20) exposed to the bacterial enrichment for 0.5, 1, 2 and 8 h. A one-way ANOVA
366 followed by the Tukey's HSD post-hoc tests were performed on the data obtained from
367 juveniles fed with enrichments from health and unhealthy *A. queenslandica*, and *R.*
368 *globostellata*.
369
370 **CEL-seq2 analysis of juvenile transcriptomes**
371 Individual juvenile *A. queenslandica* were exposed to bacterial enrichments from healthy or
372 unhealthy *A. queenslandica* (native), *R. globostellata* (foreign), or FSW for 2 or 8 h as described
373 above. At 0, 2 and 8 hpe, juveniles were individually transferred to 300 µl of RNALater (Sigma),
374 stored overnight at 4°C and then at -20°C. RNA was extracted from each juvenile using the EZ
375 Spin Column Total RNA Isolation Kit (BioBasic Inc., Toronto, Canada) according to the
376 manufacturer's instructions, and amplified and sequenced using the CEL-seq2 method [62]. The
377 CEL-seq2 samples were multiplexed, resulting in the generation of two libraries, which were
378 sequenced over two sequencing runs on an Illumina HiSeq2500, with samples from each

379 treatment group and time point divided between the two runs (S2 Table). CEL-seq2 reads were
380 processed using a publicly available pipeline (https://github.com/yanailab/CEL-Seq-pipeline)
381 and the demultiplexed raw reads were mapped to the *A. queenslandica* genome and gene-level
382 read counts were generated using Aqu 2.1 gene models [63] (S2 Table). All data are available at
383 NCBI Bioproject PRJNA1121035.
384
385 **Analysis of gene expression**
386 Differential gene expression analysis was performed with the CEL-seq2 mapped read counts
387 using the Bioconductor package DESeq2 [64]. Genes with median read counts less than 10 were
388 filtered out before analysis. Blind variance stabilizing transformation (VST) and principal
389 component analysis (PCA) was conducted on the read counts [64]. The results of the
390 unsupervised PCA analysis were visualised by a scatter plot derived from ggplot2 [65].
391 Differentially expressed genes, with adjusted p-value < 0.05, were identified by pairwise
392 comparisons between each treatment group and the corresponding FSW control. An UpSet plot
393 generated by R packages ComplexUpset and ggplot2 was utilized to visualise the number of
394 differentially expressed genes within each treatment group and the intersection across groups
395 [65,66]. Heatmaps generated by ComplexHeatmap based on inter-group normalised VST counts
396 were used to visualise the relative expression changes of differentially expressed genes [67].
397
398 Sparse partial least squares discriminant analysis (sPLS-DA), a supervised machine learning
399 method integrated into the mixOmics package [68], was used to identify expressed genes
400 featured in juveniles exposed to bacterial enrichments. The predictive model was first trained
401 using the 2 hpe datasets by repeating the 3-fold cross-validation method 50 times. Then, the
402 trained model was used to predict the bacterial type of the 8 hpe bacterial datasets, and only
403 datasets with the correct bacterial type were retained. Finally, sPLS-DA was performed on the
404 combined datasets consisting of the retained 8 hpe datasets and the full 2 hpe datasets to
405 identify feature genes for native and foreign bacteria on each principal component level. The
406 scatter plot of samples with 95% confidence ellipses generated by the R package ggplot2 based
407 on the sPLS-DA model was used to visualise the differences among treatment groups and the
408 similarities within groups. The Bioconductor package ComplexHeatmap was used to generate

409 heatmaps based on VST counts, to visualise the relative expression variations of the two PCs
410 feature genes, respectively.
411
412 A weighted co-expression analysis of gene expression profiles was undertaken using the R
413 package WGCNA [69], on VST counts obtained from DESeq2 that first were filtered by mean
414 expression and variance; VST counts of a total of 8457 genes with median or median absolute
415 deviation ranking in the top 5000 were retained. With β of 3 as soft thresholding, genes with
416 distinct expression profiles were grouped into various modules, and a weighted co-expression
417 network of the genes within the module was identified. Specifically, these networks were
418 constructed based on the signed Nowick-type of topological overlap metric, which was used to
419 cluster the modules using the dynamic tree cut algorithm with a height of 0.15 and a minimum
420 module size of 100. Co-expressed gene modules were identified by the hierarchical clustering
421 method. The relative gene expression profile of each co-expressed gene module was visualised
422 by the R package ggplot2. Module eigengenes (MEs) were correlated to bacterial treatments
423 and time points, and modules with *p*-values < 0.05 were identified as those significantly
424 correlated with the corresponding groups. ME and group relationships were visualised using
425 ggplot2 and ComplexHeatmap, respectively [65,67].
426
427 **GO and KEGG Pathway enrichment analyses**
428 The gene ontology (GO) and Kyoto Encyclopedia of Genes and Genomes (KEGG) biological
429 pathway terms of all protein coding genes were obtained by annotating the predicted
430 proteome of *A*. *queenslandica* with the online genome functional annotation tool eggNOG-
431 mapper (http://eggnog-mapper.embl.de) [70]. Enrichment analysis of KEGG pathway terms was
432 performed for each module using a one-sided version of Fisher's exact test built in the
433 Bioconductor package clusterProfiler [71]. The *p*-value was adjusted by the FDR method to
434 obtain the corresponding *q*-value, which was less than 0.05 for significantly enriched KEGG
435 pathways. Based on the results of KEGG pathway enrichment analysis, the distribution of
436 significantly enriched terms across modules was visualised with heatmaps generated by ggplot2
437 [65].
438

439 **Immunofluorescence**

440 Juveniles were fixed at 2 hpe for immunofluorescence analyses using antisera raised against
441 IRF, NF-kB and STAT peptide epitopes [72]. Rabbit polyclonal antisera against *A. queenslandica*
442 IRF (TRSGSSADEQEPERPER), STAT (QRLFNHEDDPNRNE) and NF-κB (NGIDPSSLPEALIR) peptide
443 epitopes were produced by GenScript (Piscataway, New Jersey, U.S). These antisera were
444 individually diluted 1:500 in the fresh blocking buffer and incubated with the fixed juveniles
445 overnight at 4°C as previously described [72].

446
447

448 **Acknowledgments.** The authors thank staff at the Heron Island Research Station for logistical
449 assistance during field collections, and Nick Rhodes at QCIF for management of high-
450 performance computing facilities.

451

452 **Funding.** This work was generously supported by The Australian Research Council Discovery
453 Project scheme DP170102353, DP190102521, DP230102109 (SMD, BMD) and The Gordon and
454 Betty Moore Foundation Aquatic Symbiosis Initiative 9352 (SMD). The Funders played no role in
455 the study design, data collection or analysis, decision to publish, or preparation of the
456 manuscript.

457

458 **Author contributions:**

459 Conceptualization: SMD, BMD
460 Methodology: SMD, BMD, BY, BY, HY
461 Investigation: BY, BY, HY, SMD, BMD
462 Visualization: BY, BY
463 Funding acquisition: SMD, BMD
464 Project administration: SMD, BMD
465 Supervision: SMD, BMD
466 Writing – original draft: SMD, BMD, BY
467 Writing – review & editing: SMD, BMD, BY, HY

468

469 **Competing interests.** Authors declare that they have no competing interests.

470

471 **Data and materials availability.** Transcriptomes generated by CelSeq2 as part of this study are
472 available at NCBI Bioproject PRJNA1121035. All other data are available in the main text or the
473 Supporting Information.

474

475 **References**

476

477 1. Bosch TCG. Cnidarian-Microbe Interactions and the Origin of Innate Immunity in Metazoans.
478 Annu Rev Microbiol. 2012;67: 499–518. doi:10.1146/annurev-micro-092412-155626

479 2. Bosch TCG, Blaser MJ, Ruby E, McFall-Ngai M. A new lexicon in the age of microbiome
480 research. Philos Trans R Soc B. 2024;379: 20230060. doi:10.1098/rstb.2023.0060

481 3. McFall-Ngai M, Hadfield MG, Bosch TCG, Carey HV, Domazet-Lošo T, Douglas AE, et al.
482 Animals in a bacterial world, a new imperative for the life sciences. Proc National Acad Sci.
483 2013;110: 3229–3236. doi:10.1073/pnas.1218525110

484 4. Hadfield MG, Bosch TCG. Cellular Dialogues in the Holobiont. 2020; 287–290.
485 doi:10.1201/9780429277375-17

486 5. Gilbert SF, Bosch TCG, Ledon-Rettig C. Eco-Evo-Devo: developmental symbiosis and
487 developmental plasticity as evolutionary agents. Nat Rev Genet. 2015;16: 611–622.
488 doi:10.1038/nrg3982

489 6. Bosch TCG, Guillemin K, McFall-Ngai M. Evolutionary "Experiments" in Symbiosis: The Study
490 of Model Animals Provides Insights into the Mechanisms Underlying the Diversity of Host–
491 Microbe Interactions. Bioessays. 2019;41: 1800256. doi:10.1002/bies.201800256

492 7. Dierking K, Pita L. Receptors Mediating Host-Microbiota Communication in the
493 Metaorganism: The Invertebrate Perspective. Frontiers in Immunology. 2020;11: 185–17.
494 doi:10.3389/fimmu.2020.01251

495 8. Nyholm SV, McFall-Ngai MJ. A lasting symbiosis: how the Hawaiian bobtail squid finds and
496 keeps its bioluminescent bacterial partner. Nat Rev Microbiol. 2021;19: 666–679.
497 doi:10.1038/s41579-021-00567-y

498 9. Schretter CE, Vielmetter J, Bartos I, Marka Z, Marka S, Argade S, et al. A gut microbial factor
499 modulates locomotor behaviour in Drosophila. Nature. 2018;563: 402–406.
500 doi:10.1038/s41586-018-0634-9

501 10. Hentschel U, Piel J, Degnan SM, Taylor MW. Genomic insights into the marine sponge
502 microbiome. Nat Rev Microbiol. 2012;10: 641–654. doi:10.1038/nrmicro2839

503 11. Chu H, Mazmanian SK. Innate immune recognition of the microbiota promotes host-
504 microbial symbiosis. Nat Immunol. 2013;14: 668–675. doi:10.1038/ni.2635

505 12. Alegado RA, King N. Bacterial Influences on Animal Origins. Csh Perspect Biol. 2014;6:
506 a016162. doi:10.1101/cshperspect.a016162

507 13. Woznica A, Kumar A, Sturge CR, Xing C, King N, Pfeiffer JK. STING mediates immune
508 responses in the closest living relatives of animals. eLife. 2021;10: e70436.
509 doi:10.7554/elife.70436

510 14. Richter DJ, Levin TC. The origin and evolution of cell-intrinsic antibacterial defenses in
511 eukaryotes. Curr Opin Genet Dev. 2019;58: 111–122. doi:10.1016/j.gde.2019.09.002

512 15. Nyholm SV, Graf J. Knowing your friends: invertebrate innate immunity fosters beneficial
513 bacterial symbioses. Nat Rev Microbiol. 2012;10: 815–827. doi:10.1038/nrmicro2894

514 16. Akira S, Uematsu S, Takeuchi O. Pathogen Recognition and Innate Immunity. Cell. 2006;124:
515 783–801. doi:10.1016/j.cell.2006.02.015

516 17. Bosch TCG, Adamska M, Augustin R, Domazet-Lošo T, Foret S, Fraune S, et al. How do
517 environmental factors influence life cycles and development? An experimental framework for
518 early-diverging metazoans. BioEssays. 2014;36: 1185–1194. doi:10.1002/bies.201400065

519 18. Bosch TCG, Augustin R, Anton-Erxleben F, Fraune S, Hemmrich G, Zill H, et al. Uncovering
520 the evolutionary history of innate immunity: The simple metazoan Hydra uses epithelial cells
521 for host defence. Dev Comp Immunol. 2009;33: 559–569. doi:10.1016/j.dci.2008.10.004

522 19. Silva RCMC, Gomes FM. Evolution of the Major Components of Innate Immunity in Animals.
523 J Mol Evol. 2024;92: 3–20. doi:10.1007/s00239-024-10155-2

524 20. Mansfield KM, Gilmore TD. Innate immunity and cnidarian-Symbiodiniaceae mutualism. Dev
525 Comp Immunol. 2019;90: 199–209. doi:10.1016/j.dci.2018.09.020

526 21. Williams LM, Inge MM, Mansfield KM, Rasmussen A, Afghani J, Agrba M, et al. Transcription
527 factor NF-κB in a basal metazoan, the sponge, has conserved and unique sequences, activities,
528 and regulation. Dev Comp Immunol. 2019;104: 103559. doi:10.1016/j.dci.2019.103559

529 22. Leys SP, Grombacher L, Field D, Elliott GRD, Ho VR, Kahn AS, et al. A morphological cell atlas
530 of the freshwater sponge Ephydatia muelleri with key insights from targeted single-cell
531 transcriptomes. EvoDevo. 2025;16: 1. doi:10.1186/s13227-025-00237-7

532 23. Leys SP, Hill A. Chapter one The Physiology and Molecular Biology of Sponge Tissues. Adv
533 Mar Biol. 2012;62: 1–56. doi:10.1016/b978-0-12-394283-8.00001-1

534 24. Williams LM, Gilmore TD. An innate ability: How do basal invertebrates manage their
535 chronic exposure to microbes? Plos Pathog. 2022;18: e1010897.
536 doi:10.1371/journal.ppat.1010897

537 25. Fieth RA, Gauthier M-EA, Bayes J, Green KM, Degnan SM. Ontogenetic Changes in the
538 Bacterial Symbiont Community of the Tropical Demosponge Amphimedon queenslandica:
539 Metamorphosis Is a New Beginning. Frontiers Mar Sci. 2016;3: 3022–20.
540 doi:10.3389/fmars.2016.00228

541 26. Thomas T, Moitinho-Silva L, Lurgi M, Björk JR, Easson C, Astudillo-García C, et al. Diversity,
542 structure and convergent evolution of the global sponge microbiome. Nat Commun. 2016;7:
543 11870. doi:10.1038/ncomms11870

544 27. Fan L, Reynolds D, Liu M, Stark M, Kjelleberg S, Webster NS, et al. Functional equivalence
545 and evolutionary convergence in complex communities of microbial sponge symbionts. Proc
546 National Acad Sci. 2012;109: E1878–E1887. doi:10.1073/pnas.1203287109

547 28. Gloeckner V, Wehrl M, Moitinho-Silva L, Gernert C, Schupp P, Pawlik JR, et al. The HMA-LMA
548 Dichotomy Revisited: an Electron Microscopical Survey of 56 Sponge Species. Biol Bull.
549 2014;227: 78–88. doi:10.1086/bblv227n1p78

550 29. Gauthier M-EA, Watson JR, Degnan SM. Draft Genomes Shed Light on the Dual Bacterial
551 Symbiosis that Dominates the Microbiome of the Coral Reef Sponge Amphimedon
552 queenslandica. Frontiers in Marine Science. 2016;3: 162–18. doi:10.3389/fmars.2016.00196

553 30. Ereskovsky A, Melnikov NP, Lavrov A. Archaeocytes in sponges: simple cells of complicated
554 fate. Biol Rev. 2025;100: 790–814. doi:10.1111/brv.13162

555 31. Dunn CW, Leys SP, Haddock SHD. The hidden biology of sponges and ctenophores. Trends in
556 Ecology & Evolution. 2015;30: 282–291. doi:10.1016/j.tree.2015.03.003

557 32. Musser JM, Schippers KJ, Nickel M, Mizzon G, Kohn AB, Pape C, et al. Profiling cellular
558 diversity in sponges informs animal cell type and nervous system evolution. Science. 2021;374:
559 717–723. doi:10.1126/science.abj2949

560 33. Sebé-Pedrós A, Chomsky E, Pang K, Lara-Astiaso D, Gaiti F, Mukamel Z, et al. Early metazoan
561 cell type diversity and the evolution of multicellular gene regulation. Nat Ecol Evol. 2018;2: 1–
562 17. doi:10.1038/s41559-018-0575-6

563 34. Maldonado M. Choanoflagellates, choanocytes, and animal multicellularity. Invertebrate
564 Biology. 2004;123: 1–22. doi:10.1111/j.1744-7410.2004.tb00138.x

565 35. Gaiti F, Jindrich K, Fernandez-Valverde SL, Roper KE, Degnan BM, Tanurdzic M. Landscape of
566 histone modifications in a sponge reveals the origin of animal cis-regulatory complexity. eLife.
567 2017;6: e366. doi:10.7554/elife.22194

568 36. Sogabe S, Hatleberg WL, Kocot KM, Say TE, Stoupin D, Roper KE, et al. Pluripotency and the
569 origin of animal multicellularity. Nature. 2019;570: 1–20. doi:10.1038/s41586-019-1290-4

570 37. Gauthier MEA, Pasquier LD, Degnan BM. The genome of the sponge Amphimedon
571 queenslandica provides new perspectives into the origin of Toll-like and interleukin 1 receptor
572 pathways. Evol Dev. 2010;12: 519–533. doi:10.1111/j.1525-142x.2010.00436.x

573 38. Krishnan A, Dnyansagar R, Almén MS, Williams MJ, Fredriksson R, Manoj N, et al. The GPCR
574 repertoire in the demosponge Amphimedon queenslandica: insights into the GPCR system at
575 the early divergence of animals. BMC Evol Biol. 2015;14: 270. doi:10.1186/s12862-014-0270-4

576 39. Shekarabi A, Qureishy I, Puglisi CH, Dalseth M, Vuong HE. Host–microbe interactions:
577 communication in the microbiota–gut–brain axis. Curr Opin Microbiol. 2024;80: 102494.
578 doi:10.1016/j.mib.2024.102494

579 40. Xiang X. Investigating host-symbiont crosstalk in the coral reef demosponge Amphimedon
580 queenslandica. 2021. doi:10.14264/6cdf49e

581 41. Gorp HV, Delputte PL, Nauwynck HJ. Scavenger receptor CD163, a Jack-of-all-trades and
582 potential target for cell-directed therapy. Mol Immunol. 2010;47: 1650–1660.
583 doi:10.1016/j.molimm.2010.02.008

584 42. Platanitis E, Decker T. Regulatory Networks Involving STATs, IRFs, and NFκB in Inflammation.
585 Front Immunol. 2018;9: 2542. doi:10.3389/fimmu.2018.02542

586 43. Kusiak A, Brady G. Bifurcation of signalling in human innate immune pathways to NF-kB and
587 IRF family activation. Biochem Pharmacol. 2022;205: 115246. doi:10.1016/j.bcp.2022.115246

588 44. Honda K, Taniguchi T. IRFs: master regulators of signalling by Toll-like receptors and
589 cytosolic pattern-recognition receptors. Nat Rev Immunol. 2006;6: 644–658.
590 doi:10.1038/nri1900

591 45. Glass CK, Natoli G. Molecular control of activation and priming in macrophages. Nat
592 Immunol. 2016;17: 26–33. doi:10.1038/ni.3306

593 46. Bejjani F, Evanno E, Zibara K, Piechaczyk M, Jariel-Encontre I. The AP-1 transcriptional
594 complex: Local switch or remote command? Biochim Biophys Acta (BBA) - Rev Cancer.
595 2019;1872: 11–23. doi:10.1016/j.bbcan.2019.04.003

596 47. Sebé-Pedrós A, Mendoza A de, Lang BF, Degnan BM, Ruiz-Trillo I. Unexpected repertoire of
597 metazoan transcription factors in the unicellular holozoan Capsaspora owczarzaki. Molecular
598 Biology and Evolution. 2011;28: 1241–1254. doi:10.1093/molbev/msq309

599 48. Gauthier M, Degnan BM. The transcription factor NF-κB in the demosponge Amphimedon
600 queenslandica: insights on the evolutionary origin of the Rel homology domain. Dev Genes Evol.
601 2008;218: 23–32. doi:10.1007/s00427-007-0197-5

602 49. Williams LM, Gilmore TD. Looking Down on NF-κB. Mol Cell Biol. 2020;40: e00104-20.
603 doi:10.1128/mcb.00104-20

604 50. Srivastava M, Simakov O, Chapman J, Fahey B, Gauthier MEA, Mitros T, et al. The
605 Amphimedon queenslandica genome and the evolution of animal complexity. Nature.
606 2010;466: 720–726. doi:10.1038/nature09201

607 51. Maritan E, Quagliariello A, Frago E, Patarnello T, Martino ME. The role of animal hosts in
608 shaping gut microbiome variation. Philos Trans R Soc B. 2024;379: 20230071.
609 doi:10.1098/rstb.2023.0071

610 52. Honda K, Ohba Y, Yanai H, Negishi H, Mizutani T, Takaoka A, et al. Spatiotemporal regulation
611 of MyD88–IRF-7 signalling for robust type-I interferon induction. Nature. 2005;434: 1035–1040.
612 doi:10.1038/nature03547

613 53. Ikushima H, Negishi H, Taniguchi T. The IRF Family Transcription Factors at the Interface of
614 Innate and Adaptive Immune Responses. Cold Spring Harbor Symposia on Quantitative Biology.
615 2014;78: 105–116. doi:10.1101/sqb.2013.78.020321

616 54. Fitzgerald KA, Kagan JC. Toll-like Receptors and the Control of Immunity. Cell. 2020;180:
617 1044–1066. doi:10.1016/j.cell.2020.02.041

618 55. Ahmad Z, Kahloan W, Rosen ED. Transcriptional control of metabolism by interferon
619 regulatory factors. Nat Rev Endocrinol. 2024;20: 573–587. doi:10.1038/s41574-024-00990-0

620 56. Thomas T, Rusch D, DeMaere MZ, Yung PY, Lewis M, Halpern A, et al. Functional genomic
621 signatures of sponge bacteria reveal unique and shared features of symbiosis. 2010;4: 1557–
622 1567. doi:10.1038/ismej.2010.74

623 57. Ueda N, Richards GS, Degnan BM, Kranz A, Adamska M, Croll RP, et al. An ancient role for
624 nitric oxide in regulating the animal pelagobenthic life cycle: evidence from a marine sponge.
625 Sci Rep. 2016;6: 37546. doi:10.1038/srep37546

626 58. Say TE, Degnan SM. Molecular and behavioural evidence that interdependent photo - and
627 chemosensory systems regulate larval settlement in a marine sponge. Mol Ecol. 2020;29: 247–
628 261. doi:10.1111/mec.15318

629 59. Degnan BM, Adamska M, Richards GS, Larroux C, Leininger S, Bergum B, et al. Porifera.
630 Springer Vienna; 2015. pp. 65–106. doi:10.1007/978-3-7091-1862-7_4

631 60. Larroux C, Fahey B, Adamska M, Richards GS, Gauthier M, Green K, et al. Whole-Mount In
632 Situ Hybridization in Amphimedon. Cold Spring Harb Protoc. 2008;2008: pdb.prot5096.
633 doi:10.1101/pdb.prot5096

634 61. Sogabe S, Nakanishi N, Degnan BM. The ontogeny of choanocyte chambers during
635 metamorphosis in the demosponge Amphimedon queenslandica. EvoDevo. 2016;7: 6.
636 doi:10.1186/s13227-016-0042-x

637 62. Hashimshony T, Senderovich N, Avital G, Klochendler A, Leeuw Y de, Anavy L, et al. CEL-
638 Seq2: sensitive highly-multiplexed single-cell RNA-Seq. Genome Biol. 2016;17: 77.
639 doi:10.1186/s13059-016-0938-8

640 63. Fernandez-Valverde SL, Calcino AD, Degnan BM. Deep developmental transcriptome
641 sequencing uncovers numerous new genes and enhances gene annotation in the sponge
642 Amphimedon queenslandica. BMC Genomics. 2015;16: 720–11. doi:10.1186/s12864-015-1588-
643 z

644 64. Love MI, Huber W, Anders S. Moderated estimation of fold change and dispersion for RNA-
645 seq data with DESeq2. Genome Biol. 2014;15: 550. doi:10.1186/s13059-014-0550-8

646 65. Wickham H. ggplot2, Elegant Graphics for Data Analysis. R. 2016. doi:10.1007/978-3-319-
647 24277-4

648 66. Lex A, Gehlenborg N, Strobelt H, Vuillemot R, Pfister H. UpSet: Visualization of Intersecting
649 Sets. IEEE Trans Vis Comput Graph. 2014;20: 1983–1992. doi:10.1109/tvcg.2014.2346248

650 67. Gu Z, Eils R, Schlesner M. Complex heatmaps reveal patterns and correlations in
651 multidimensional genomic data. Bioinformatics. 2016;32: 2847–2849.
652 doi:10.1093/bioinformatics/btw313

653 68. Rohart F, Gautier B, Singh A, Cao K-AL. mixOmics: An R package for 'omics feature selection
654 and multiple data integration. PLoS Comput Biol. 2017;13: e1005752.
655 doi:10.1371/journal.pcbi.1005752

656 69. Langfelder P, Horvath S. WGCNA: an R package for weighted correlation network analysis.
657 BMC Bioinform. 2008;9: 559–559. doi:10.1186/1471-2105-9-559

658 70. Cantalapiedra CP, Hernández-Plaza A, Letunic I, Bork P, Huerta-Cepas J. eggNOG-mapper v2:
659 Functional Annotation, Orthology Assignments, and Domain Prediction at the Metagenomic
660 Scale. Mol Biol Evol. 2021;38: 5825–5829. doi:10.1093/molbev/msab293

661 71. Wu T, Hu E, Xu S, Chen M, Guo P, Dai Z, et al. clusterProfiler 4.0: A universal enrichment tool
662 for interpreting omics data. Innov. 2021;2: 100141. doi:10.1016/j.xinn.2021.100141

663 72. Yang B, Degnan BM, Degnan SM. An improved whole-mount immunofluorescence protocol
664 for juvenile Amphimedon queenslandica v1. 2024.
665 doi:10.17504/protocols.io.e6nvw1o2wlmk/v1

666